HHS Public Access

Author manuscript

Nat Mater. Author manuscript; available in PMC 2017 July 19.

Published in final edited form as:

Nat Mater. 2016 July ; 15(7): 792–801. doi:10.1038/nmat4586.

Directed migration of cancer cells by the graded texture of the underlying matrix

JinSeok Park[1,2,5], **Deok-Ho Kim**[3], **Hong-Nam Kim**[4], **Chiaochun Joanne Wang**[5], **Moon Kyu Kwak**[4], **Eunmi Hur**[5], **Kahp-Yang Suh**[4], **Steven S. An**[6,7,8,*], and **Andre Levchenko**[1,2,*]

[1]Department of Biomedical Engineering, Yale University, New Haven, CT 06520, USA.

[2]Yale Systems Biology Institute, Yale University, West Haven, CT 06516, USA

[3]Department of Bioengineering, University of Washington, Seattle, WA 98195, USA.

[4]Department of Mechanical & Aerospace Engineering, Seoul National University, Seoul, Republic of Korea

[5]Departments of Biomedical Engineering, The Johns Hopkins University School of Medicine, Baltimore, MD 21205, USA.

[6]Department of Environmental Health Sciences, Johns Hopkins Bloomberg School of Public Health, Baltimore, MD 21205, USA.

[7]Department of Chemical and Biomolecular Engineering, The Johns Hopkins University, Baltimore, MD 21218, USA.

[8]Physical Sciences-Oncology Center, Johns Hopkins University, Baltimore, MD 21218, USA.

Abstract

Living cells and the extracellular matrix (ECM) can display complex interactions that define key developmental, physiological and pathological processes. Here, we report a new type of directed migration — which we term ‘topotaxis’ — by which cell movement is guided by the gradient of the nanoscale topographic features in the cells’ ECM environment. We show that the direction of topotaxis is reflective of the effective cell stiffness, and that it depends on the balance of the ECM-triggered signalling pathways PI3K-Akt and ROCK-MLCK. In melanoma cancer cells, this balance can be altered by different ECM inputs, pharmacological perturbations or genetic alterations, particularly a loss of *PTEN* in aggressive melanoma cells. We conclude that topotaxis is a product of the material properties of cells and the surrounding ECM, and propose that the invasive capacity of many cancers may depend broadly on topotactic responses, providing a potentially attractive mechanism for controlling invasive and metastatic behaviour.

*To whom correspondence should be addressed: Steven S. An, Ph D. (san@jhu.edu), Andre Levchenko, Ph.D. (andre.levchenko@yale.edu).

Author contributions

J.P and A.L. conceived and designed the project. J.P performed the experiments. D.K, H.K and M.K.K designed and fabricated substrata under the supervision of A.L. and K.Y.S. J.P and E.H tracked and analyzed migration time-lapse data. C.J.W transfected plasmids and made cell lines. A.L and S.S.A supervised the project. J.P and A.L wrote the manuscript. A.L and S.S.A reviewed and revised the manuscript.

Living cells have evolved a range of mechanisms to recognize a diverse set of environmental cues, including those present in spatially graded doses. For instance, in addition to being sensitive to spatial gradients of various dissolved chemical factors (chemotaxis)[1], many eukaryotic cell types can detect gradients in the chemical or physical properties of the cell adhesion substratum, such as the graded density of the surface-bound extracellular matrix proteins (haptotaxis)[2,3] or graded substratum rigidity (durotaxis)[4,5]. Within these gradients, individual cells can migrate towards higher ECM densities or stiffer areas of the substratum. Our understanding of the mechano-chemical guidance cues associated with adhesion substrata comes mostly from studies, in which the cell substratum is defined to be flat and featureless. However, the more native, *in vivo* cell adhesion surfaces are topographically more complex, primarily due to a large diversity of ECM features spanning multiple scales of size and organization. For example, collagen fibrils and fibers interlinked within complex matrices are exemplary of this 3D topographic complexity[6].

A convenient way to mimic and study the effects of complex ECM topographies, while retaining the advantages of essentially 2D experimentation, is to use quasi-3D, nano-patterned surfaces, capturing the *in vivo* geometry and size ranges of large ECM fibers. In our prior analysis, we found that many types of mammalian cells have the ability not only to anisotropically orient their migration and polarization in contact with ridged nano-topographic structures[7-10], but also to detect and respond to gradients of these nano-scale features by biasing their directional migration[11,12]. This novel phenomenon of single cell sensitivity to the topography gradient, also reported on micro-scale[13], which we will term here “topotaxis”, is still poorly understood. In particular, it is not clear whether it is a version of more accepted haptotaxis and durotaxis processes, or if it is distinct from them in some essential way. Furthermore, the molecular basis of topotaxis is still not explored. Finally, it has not been addressed whether there is a potential for topotaxis to affect the invasive behavior of cancer cells interacting with the surrounding ECM. We thus set out to examine topotaxis in the context of one of the most invasive cancers, melanoma.

Melanoma, an aggressive cancer mostly affecting the skin, results in the highest percentage of skin cancer related deaths[14]. Melanoma cells can develop from more benign radial growth patterns to more invasive, vertical growth[14]. In the latter case, cell invasion takes place through the dermis, a collagen-rich and cell-poor layer of connective tissue. Within dermis, collagen fibers are highly organized and frequently aligned, presenting an organized ECM-based adhesion substratum. As cancer cells migrate through the collagen matrix, they frequently express proteins, such as matrix metalloproteinases (MMPs), that can break down collagen fibers, which can cause the inhomogeneous density in the matrix and generate arrays of severed fiber bundles[15,16]. Melanoma cells and resident fibroblasts can also deposit matrix components, with fibronectin, which is essential for invasive cell migration[17,18].

Increasing melanoma invasiveness is frequently associated with a range of genetic changes, one of which is a loss of functional PTEN, which can lead to over-activation of PI3K-Akt signaling pathway[14]. Although this pathway has been associated with controlling cell migration, how it can influence melanoma invasiveness is currently unknown. Here, we provide evidence for topotaxis of melanoma cells, and show that it depends on the material

properties of both the model matrix environment (density and structure) and the cell itself (stiffness). Genetic changes, such as loss of PTEN and the local density of ECM can determine the directionality of topotaxis-driven cell migration. In particular, we show that there exist conditions under which more aggressive melanoma cells can shift in the direction of sparser quasi-3D matrix, modeling the *in vivo* ECM features, whereas, strikingly, non-invasive melanoma cells shift in the opposite direction. We suggest a model accounting for this behavior and show that, in agreement with model predictions, the manipulation of the PI3K-Akt or ROCK-MLCK dependent signaling pathways can determine the direction of the topotactic movement. The results have important implications for understanding the interplay between genetic mutations associated with cancer aggressiveness and the invasive properties of the cells. The results can also account for basic mechanisms underlying topotaxis in different cell types, and underscore the importance of accounting for materials properties of cells and their micro-environment in understanding physiological and pathological processes.

Topotaxis of melanoma guided by the gradient of post density

To examine topotactic properties of melanoma cells, we used capillary force lithography to fabricate arrays of nano-scale posts with graded post density. We refer to these arrays as graded post density arrays (GPDA). GPDAs had the gradient of post spacing in one of the orthogonal directions (*x* direction in Fig. 1a), with the density varying between 0.3 and 4.2 μm, and constant spacing (600 nm) in the other direction (*y* direction in Fig. 1a). Each post was 600 nm in diameter, within the range of natural collagen fiber (from 50 nm to 20 μm)[6,19,20] was then coated with fibronectin (FN) to focus on the matrix component essential for invasive migration, and melanoma cells were plated on the surface (Fig. 1a and Supplementary Fig. 1). Since the scale of single cell is one order of magnitude larger than that of the nano-posts, such anisotropic nanotopography can present a directional physical cue to a cell attached on to the substrata. Invasive 1205Lu melanoma cells adhering to this substratum displayed spreading and active migration, similar to their overall behavior on flat adhesion substrata. However, individual cells also frequently exhibited distinct organization of membrane protrusions, depending on the local post density: long/parallel filopodia on sparser post density side and short/randomly oriented, thicker protrusions on denser post density side (Fig. 1b). The bundles of long and parallel filopodia observed on sparser density side are similar to those found at the leading edge of cells undergoing directional migration[21]. This result was consistent with the possibility of topotactic cell behavior, which we directly explored next.

We tracked the biased shift in the location of invasive (1205Lu) and non-invasive (SBcl2) melanoma cells lines on GPDAs coated with FN at two distinct densities, 10 and 50 μg/ml, for 3 days. In particular, we explored if cells would accumulate in the sparser or denser areas of the substratum. Interfacing with denser arrays of posts can present cells with both higher overall amount of ECM and a less deformable, thus, more effectively rigid surfaces. Therefore, both haptotactic and durotactic mechanisms of cell migration would predict that cells might accumulate over time in denser parts of the substratum[12,13]. Surprisingly, in contrast to this prediction, we observed that both cell lines accumulated in sparser areas, if the surface was pre-coated with 10 μg/ml of FN (Fig. 1c and Supplementary Fig. 2). At 50

μg/ml of FN, the results were divergent, with 1205Lu cells accumulating in the sparser array areas, whereas SBcl2 cells accumulating in the denser array zones. These results could only be accounted by directed cell migration. Cell proliferation for individual cell lines was independent of the post density, although invasive cells proliferated faster than non-invasive cells, particularly on lower FN density (Supplementary Fig. 3).

To investigate whether this biased accumulation results from a directional migration mechanism and to explore its generality in other cell types, we then tracked live cells for a much shorter time of 5 hours, which allowed to perform continuous live cell imaging. Consistent with the results above (Fig. 1c), we found for two invasive melanoma cell lines examined, 1205Lu and WM983B, that cells migrated toward sparser post array zones of GPDA pre-coated with 10 and 50 μg/ml of FN, again suggesting that this topotactic cellular migration was guided by a mechanism distinct from haptotaxis or durotaxis (Figs. 1d,e). The direction of topotactic migration of two non-invasive melanoma cell lines, SBcl2 and WM1552, was again FN density dependent. These cells exhibited directional cell migration opposite to that of invasive cells (i.e. toward dense post array zones on GPDA) on surfaces pre-coated with 50 μg/ml of FN; however, on GPDA pre-coated 10 μg/ml of FN, they switched the migration directionality and shifted from dense to sparse array zones (the same direction as their invasive counterparts) (Figs. 1d,e). These results suggest that the melanoma cells are highly sensitive to the gradient of the density of topographic features, and that this topotactic behavior is not equivalent to either haptotactic or durotactic directed cell guidance.

Invasive melanoma cells migrate from denser to sparser areas

We confirmed that 1205Lu melanoma cells showed significant biased topographic shifts, with a broad distribution of single cell trajectories on GPDAs pre-coated with 10 and 50 μg/ml of FN (Fig. 2a). We also found that the migration bias was at least partially accounted for by a bias in motility persistence (Supplementary Fig. 4). We then used high resolution cell imaging to address putative mechanisms of the topotactic migration. In particular, we examined the possibility that topotaxis results from the differential ability of individual cells to conform to the topography of the underlying substratum. Cells whose plasma membrane-associated cortical cytoskeleton is relatively stiff can, as a consequence, have less deformable membranes[22-24], not capable of full penetration into the areas separating the nano-posts, thus being unable to fully conform to the shapes of the gaps between topographic features. Hence, this limited membrane deformability could lead to a decreased overall contact between the plasma membrane and the substratum-bound ECM. In the extreme, it can prevent contact with the lateral post surfaces, i.e. essentially localizing spreading cells only to the tops of the posts. On the other hand, cells with less stiff cortical cytoskeleton and thus more deformable membranes might successfully envelop the posts and spaces between them, thus increasing their exposure to ECM. Of course, this differential ability to conform to the complex surface topography depends on the features of the topography itself, e.g., the local spacing between the posts. To explore this conceptual model, we first directly addressed the possibility of differential cell penetration into the inter-post spaces by high resolution 3D imaging the focal adhesion (FA) complexes. We found that FA complexes (indicating the location of cell-ECM interfaces) indeed displayed

differential depth of penetration into the inter-post spaces in the sparser vs. denser areas of GPDA (Figs. 2b,c). Furthermore, scanning electron microscopy imaging suggested presence of pseudopods between posts in sparser but not denser areas (Supplementary Fig. 5a). As a result of differential penetration, cells migrating towards areas maximizing their ECM contact would be expected to migrate to lower post densities for softer cells, consistent with the experimental observations and thus supporting the conceptual model of topotaxis.

Although cell stiffness may be an inherent property of a specific cell type, it may also depend on the input from the cell adhesion substratum, and in particular the local density of the topographic features. To explore this possibility, we directly measured effective stiffness of the cortical cytoskeleton and the associated plasma membrane[25,26]. Specifically, we examined micro-rheological properties of 1205Lu cells by magnetic twisting cytometry, using RGD-coated beads bound to the integrin receptors on the cell surfaces. We analyzed displacements of these beads in response to magnetic forces, which allowed us to determine the effective resistance of these beads to forces displacing them and thus to evaluate cell stiffness and its dependence on the local post density. Interestingly, the effective stiffness values of 1205Lu cells were significantly lower in the sparser post zones, compared to the values found in denser zones (Fig. 2d). This result suggested that, both due to a lower cell stiffness and increased inter-post distances, 1205Lu cell-ECM contact can be relatively more extensive in the lower vs. higher post density zones, consistent with the model connecting the direction of the topotactic motility with the ability to conform to the topographic features of the cell adhesion substratum.

PI3K vs. ROCK signaling determines topotaxis direction

What can account for the dependence of the cell stiffness on the post density? It is generally accepted that the cortical cytoskeleton can increase its apparent stiffness as a function of enhanced cross-linking of actin polymers due to augmented myosin activity[27]. Myosin can in turn be regulated by phosphorylation of the myosin light chain (MLC) by the MLC kinase (MLCK). MLCK activity is regulated by elevated activation of the small GTPase RhoA causing up-regulation of the activity of the RhoA-dependent kinase (ROCK)[28-30]. RhoA activity can be triggered by an increased ECM engagement by integrin receptors, and thus be enhanced by more extensive cell-ECM contact. We indeed found that MLC phosphorylation was correlated with the density of FN in 1205Lu cells (Fig. 2e). It thus seemed paradoxical that the stiffness of 1205Lu cells would decrease rather than increase on sparser post array, where the cell-substratum contact is expected to be higher. However, this paradox can be resolved if another signaling pathway triggered by ECM acts to counteract the effects of ECM-activated RhoA-ROCK-MLCK pathway. One such pathway operates through the activation of another small GTPase, Rac1, frequently accompanied by elevated activity of PI3K[31,32]. We indeed found that, in 1205Lu cells, an increasing engagement of FN triggered progressively higher PI3K activation in an ECM dose dependent fashion, as evaluated by phosphorylation of the downstream kinase Akt (Fig. 2e). These results thus suggested that both ROCK and PI3K signaling can be enhanced by ECM, with the potential for opposing effects on the membrane protrusion and effective stiffness. Furthermore, we found evidence for negative cross-regulation between ROCK and PI3K that could enhance this effect (Supplementary Fig. 6). For 1205Lu cells, the effect of PI3K could dominate that of ROCK,

thus leading to decreasing rather than increasing effective membrane stiffness with decreasing post density (Fig. 2f). Based on these observations, we tested this model in the next set of experiments.

If the directionality of topotaxis is defined by differential control of cell stiffness, which in turn depends on the ECM regulated interplay between PI3K and ROCK-activated pathways, pharmacological perturbations of these pathways are expected to affect topotaxis properties (Fig. 3a). In particular, a sufficiently strong inhibition of PI3K signaling pathway could allow the ROCK-activated pathway to dominate the outcome (Fig. 3a). This could lead to a reversal of the stiffness dependence on the post density, and thus could in turn reverse the direction of the topotactic cell displacement. Indeed, we observed that PI3K inhibition reversed the directionality of topotactic motility of 1205Lu cells, at both 10 and 50 μg/ml of FN coating density (Figs. 3b,c and Supplementary Fig. 4). In agreement with the model above, the cell stiffness profile was also reversed by PI3K inhibition, with the higher cell stiffness values now observed at the sparser density zones of the post arrays (Fig. 3d). However, inhibition of ROCK did not change either the direction of topotaxis or stiffness profile, regardless of FN coating density (Figs. 3e-g), also in agreement with the model (Fig. 3a).

Our topotaxis model also implied that, due to differential contact with ECM across the length of a single cell, PI3K activity is expected to be polarized. Notably, spatially localized PI3K activation has been associated with directional migration in different cell types[1,33,34]. To directly assess local PI3K activity, we transfected cells with 3-phosphoinotitide-specific Akt pleckstrin-homology domain fused with fluorescent protein (mRFP in 1205Lu or GFP in SBcl2), thus directly tracking PI3K activity in individual cells. We indeed observed that spatial localization of PI3K signaling in individual 1205Lu cells was polarized toward sparser post arrays, where effective membrane stiffness decreases (Supplementary Fig. 7).

PTEN reverses topotaxis of non-invasive melanoma

The dominance of PI3K activity over RhoA-ROCK-MLCK signaling may be a specific characteristic of invasive melanoma cell lines, such as 1205Lu, known to have a loss of functional PTEN, a PI3K antagonist[14]. We confirmed that these cell lines had elevated basal levels of Akt phosphorylation compared to non-invasive SBcl2 and WM1552C cells (Fig. 4a). Conversely, the activity of ROCK was relatively higher in the non-invasive cells, suggesting a change in the relative balance of both PI3K and ROCK pathways, affecting the cell stiffness and protrusive activity. In spite of this pathway ‘rebalancing’, we found that both PI3K and ROCK activities again correlated with the surface FN density (Fig. 4b). Using these data, we predicted that PI3K dominance over ROCK signaling would occur in SBcl2 cells at low but not high ECM density (Fig. 4c), explaining the reversal of topotactic direction in non-invasive compared to invasive cells at 50 μg/ml, but not at 10 μg/ml (Figs. 1d,e and 4d). This explanation was further supported by the reversal of the dependency of the cell stiffness on the post density and of the spatially bias of PI3K signaling toward denser post regions in SBcl2 vs. 1205Lu cell lines, observed at high but not low FN coating density (Fig. 4e and Supplementary Fig. 7c). These results suggested that the stiffness of non-invasive cells at higher ECM density values can be such that they would display

essentially no penetration in the inter-post spaces. Furthermore, these results imply that increasing inter-post distance, which might have gradually become more permissive for inter-post membrane protrusion, is compensated in these cells at high ECM density by increasing cell stiffness, ensuring that cells essentially remain at the top of the posts at any post density. We indeed found that, whereas at 10 μg/ml of FN the penetration of the plasma membrane (as evaluated by FA confocal microscopy imaging) was similar to that found in 1205Lu cells, at 50 μg/ml of FN the average penetration was close to zero (Figs. 4f, g). In addition, in contrast to non-invasive cells cultured on GPDA pre-coated with 10 μg/ml of FN and invasive cells on both examined FN densities, which showed differential vertical penetration of pseudopods, pseudopods of SBcl2 on 50 μg/ml of FN pre-coated GPDA were exclusively found on the tops of posts, independent of the post density, suggesting very limited penetration between posts (Supplementary Fig. 5b).

To further confirm the role of differential balancing between PI3K and ROCK pathways in defining topotactic migration in the non-invasive SBcl2 cell line, we explored the effect of pharmacological perturbations of these pathways. In this case, PI3K inhibition was predicted to enhance the reversal of topotactic migration of SBcl2 cells vs. 1205Lu cells, so that the direction would be now reversed at both high and low FN coating densities, permitting consistent cell displacement from lower to higher post density areas. Inhibition of ROCK, on the other hand, was predicted to abolish the relative migration reversal and to induce directed migration from denser to sparser zones at all FN coating densities (Fig. 5a). These effects were indeed observed (Figs. 5b-g). Furthermore, the directionality of topotactic migration was again consistent with the effect of pharmacological perturbations on how cell stiffness or persistence of cell migration depended on post and ECM density (Figs. 5d,g and Supplementary Fig. 4). Finally, to mimic genetic loss of PTEN, expected to enhance PI3K activity and potentially suppress ROCK activity, we pharmacologically inhibited this phosphatase. As expected in accordance with our model, non-invasive SBcl2 and WM1552 cells, at 50 μg/ml of FN, showed topotactic migration from dense to sparse areas of the post array, thus now showing topotaxis directionality consistent with that of invasive cell (Figs. 5h,i).

Outlook

Oriented cell motility in gradients of topographic features, termed here ‘topotaxis’, has remained largely unexplained. The data presented in this study suggest a mechanism that strongly depends on the ability of the plasma membrane and the underlying cortical cytoskeleton to conform to the topographic complexity of the cell adhesion substratum. The complex substratum topographies can be a reflection of the ECM structure in the cell vicinity, composed of both intact and potentially severed fibers, interlinked around a cell in a complex meshwork. Our analysis suggests that a gradient of density of such topographic features can be differentially interpreted by a cell as either attractive or repulsive, depending on whether the cell forms ECM contacts only due to exploration of the immediate surfaces of the topographic features (e.g., the tops of the posts in this study), or it enhances the ECM contact by penetrating into spaces separating these features (e.g., exploring inter-post spaces in this study). We found that this differential ability to conform to the topographic complexity was a function of the genetic differences naturally present in melanoma cells of

different degrees of invasiveness, as well as the signaling activity triggered by engagement of ECM. Importantly, both genetic and signaling inputs affected the same signaling circuit, involving PI3K and ROCK dependent pathways, which in turn regulated the effective stiffness of the cortical cytoskeleton and the plasma membrane and thus directionality of topotaxis.

In spite of its apparent complexity, the mechanism of topotaxis is easily generalized to three possible classes of cell interactions with topographically complex ECM environment. If a cell is either fully compliant with the ECM topography (can fully envelop ECM fibers) or is fully non-compliant (is localized on the tops of ECM fibers, being incapable to envelop them), the guidance effect of a graded ECM topography is similar to the haptotactic guidance, in which cells are expected to migrate up the gradient of ECM density, and thus higher density of topographic features. However, if the cell has an intermediate compliance, it may have higher ECM penetration and thus ECM contact in sparser rather than denser matrix zones, which can guide its migration from denser to sparser feature zones. Cell compliance to the matrix structure is a function of the cell stiffness, which in turn can be a function of ECM triggered signaling activity, resulting in a feedback control of topotactic migration. Interestingly, this conceptual model allows for the possibility that even the same topography gradient can specify opposite migration directions. This has been observed to occur when fibroblasts undergo topotaxis in two opposite directions on the same ECM topography gradient, migrating towards an optimum ECM fiber density (i.e., converging away from very sparse or very dense areas)[11]. In this case the fibroblasts are predicted to be fully compliant in the sparser ECM zones and only partially compliant in denser ECM areas.

Membrane stiffness and thus cell compliance to the topographic features of the surrounding matrix and, ultimately, the topotaxis direction, are found here to depend on a specific signaling network architecture, in which two parallel signaling pathways, both triggered by the ECM-integrin engagement have opposite effects on the cortical cytoskeleton and the effective membrane stiffness. Thus, the stiffness value or, conversely, protrusive activity of the plasma membrane, is a result of a balance of activities in these pathways. With increasing dominance of PI3K-Akt activity, the stiffness value decreases and thus membrane compliance to the matrix topography can increase (Fig. 6a). Conversely, if ROCK-MLCK pathway activity dominates, the membrane stiffness can increase, limiting compliance to the topographic features (Fig. 6b). Relative balance of signaling activities in these pathway, such as PI3K and its antagonist, PTEN, can shift across the length of a single cells which is expected to orient directional cell migration[35,36]. Thus, as observed in this study, locally polarized PI3K activity biased by inhomogeneous cell-ECM contact could help explain topotactic migration on a single cell level. As demonstrated in this study, both genetic and pharmacological perturbations of PI3K and ROCK-MLCK signaling pathways can change their relative dominance, and switch the directionality of topotactic migration. Interestingly, this signaling network architecture is structurally similar to the one proposed to account for chemotactic cell migration (the so-called LEGI network)[1,37], suggesting that similar principles underlie the control of distinct tactic mechanisms.

The mechanism of topotaxis proposed here emphasizes intimate interdependence of the matrix structure and the activity of the signaling networks controlling cell mechanics. This

framework can provide a unifying view of the effects of different genetic mutations implicated in progression from non-invasive to invasive cell behavior. For instance, the loss of PTEN is frequently observed in transition of cancer cells to aggressive and invasive growth, but the exact reason for this switch in cell phenotype is not clear. Furthermore, it has been shown in mouse models that a gradual decrease in PTEN gene dosage progressively increasing the ability of melanoma cells and normal melanocytes to penetrate extracellular matrix[38]. The topotaxis model proposed here strongly suggests that the increased dominance of the PI3K-Akt signaling pathway precipitated by the loss of PTEN leads to an increased cell compliance and topotaxis from dense to sparse matrix areas. Since cancer invasion is also frequently accompanied by partial degradation of ECM due to an increased expression of MMPs, migration from denser to sparser matrix areas can enhance the ability of the cells to shift to the areas of sparser and, possibly more aligned matrix fibers, enabling more directed and efficient aggressive spread. Loss of PTEN may enhance MMP secretion thus additionally contributing to this process[39]. On the other hand, less aggressive cells, expressing functional PTEN, would be less compliant, which can direct their topotactic migration into denser matrix areas, complicating migratory behavior, even if matrix is partially degraded. Many other genetic alterations could potentially affect cell stiffness, either through the ECM regulated PI3K-Akt and ROCK-MLCK signaling pathways, or through other mechanisms, accounting for increased invasive behavior. Compliance with the complex substratum topography can also influence formation of focal adhesions of different size and maturity, which might also contribute to the topotaxis control[40]. Conveniently, this network-based view can also suggest multiple potential interventions that may help shift signaling activity and alter cell stiffness thus reversing aggressive phenotypes.

Our analysis illustrates the importance of changing the prevailing emphasis on cell analysis on flat adhesion substrata, where various tactic phenomena have been described so far, to more complex but also more realistic environments, in which the haptotactic, durotactic and topotactic guidance effects can be intertwined. Studies of cell migrations on nano-structured surfaces also suggested that cells may actively sense the rigidity of local micro-environment[41,42]. The initial analysis undertaken here, with the assistance of tools that are more complex than the 2D environment of the Petri dish, but less daunting than the 3D environments found in many tissues, can help establish the framework for quantitative description of the mechanical and chemical properties of both extracellular matrix and of the live cells actively interacting with it.

Methods

Fabrication of Topographical Pattern Arrays

To construct graded post density array (GPDA), poly(urethane acrylate) (PUA) was used as a mold material from the silicon master as previously described (Supplementary Fig. 1)[46]. Briefly, the ultraviolet (UV)-curable PUA was drop-dispensed onto a silicon master and then a flexible and transparent polyethylene terephthalate (PET) film was brought into contact with the dropped PUA liquid. Subsequently, it was exposed to UV light (λ= 200-400 nm) for 30 s through the transparent backplane (dose = 100 mJ cm^{-2}). After UV curing, the mold was peeled off from the master and additionally cured overnight to terminate the remaining

active acrylate groups on the surface prior to use as a first replica. The resulting PUA mold used in the experiment was a thin sheet with a thickness of ~50 μm.

The topographic patterns with variable local density and anisotropy were fabricated on glass coverslips, using UV-assisted capillary molding techniques[47]. Prior to application of the PUA mold, the glass substratum was cleaned with isopropyl alcohol, thoroughly rinsed in distilled ionized water, and then dried in a stream of nitrogen. Subsequently, an adhesive agent (phosphoric acrylate: propylene glycol monomethyl ether acetate = 1:10, volume ratio) was spin-coated to form a thin layer (~100 nm) for 30 s at 3000 rpm. A small amount of the same PUA precursor was drop-dispensed on the substrate and a PUA mold was directly placed onto the surface. The PUA precursor spontaneously filled the cavity of the mold by means of capillary action and was cured by exposure to UV light (λ= 250-400 nm) for ~30 s through the transparent backplane (dose = 100 mJ cm^{-2}). After curing, the mold was peeled off from the substrate using a sharp tweezers. Patterns were viewed and photographed with a LEO FESEM 1530 operating at 1 kV. The nanopost array used in this study, GPDA, has the post spacing gradient along the x direction and post spacing to the y direction, resulting in an anisotropic density gradient. Thus the nano-posts used had a constant diameter of 600 nm with the varying post-to-post spacing from 300 nm [spacing ratio (spacing/diameter) of 0.5] to 4.2 μm (spacing ratio of 7) in the x direction, but constant post-to-post spacing of 600 nm (spacing ratio of 1) to the y direction.

Cell Culture

We used several cell lines from the Wistar Institute collection: 1205Lu, WM983B, SBcl2 and WM1552, a gift from Dr. Rhoda Alani (Boston University). We also used 1205Lu and SBcl2 with the transfected with plasmids coding for 3-phosphoinotitide-specific Akt pleckstrin-homology domain fused with mRFP in 1205Lu or GFP in SBcl2. We transfected mRFP-Akt PH plasmid in 1205Lu and GFP-Akt PH plasmid in SBcl2 using lipofectaminTM 2000 transfection reagents (Thermo Fisher, 11608027) as described in product's manual. mRFP and GFP-Akt PH plasmids were gifted by Dr. Jin Zhang's lab (UCSD)[48]. After cloning Akt PH domain from GFP-Akt PH plasmids, we ligated the mRFP plasmid to it. The cells were cultured in Dulbecco's modified Eagle's medium (Gibco) supplemented with 10% fetal bovine serum (Gibco), 50 U/ml penicillin, and 50 μg/ml streptomycin (Invitrogen) at 37°C, 5% CO_2 and 90% humidity. These were splited 1:4 after trypsinization every 2-3 days. Glass coverslip with the topographical pattern substratum was previously glued onto the bottom surface of the custom-made MatTek dish (P35G-20-C). Then, we replated cells on the pattern pre-coated by 10 or 50 μg/ml of fibronectin (Sigma-Aldrich, F1141) for 3 hours and incubate up to 12 hours for the attachment. For the perturbation of signaling pathway related to cell migration, 5 μM of Y27632 (Sigma-Aldrich, Y0503), 10 μM of LY294002 (Sigma-Aldrich, L9908) and 100nM of bpV(HOpic) (Sigma-Aldrich, SML0884) were added. Mycoplasma contamination was tested with Hoescht (Invitrogen, 33342).

Western Blot Analysis

Cells are homogenized in RIPA buffer (Thermo Scientific®) with protease inhibitor cocktail (Thermo Scientific®), then centrifuged at 12,000 × g at 4 °C for 30 min. The supernatant

was collected and protein was quantified using Bradford assay kit (Pierce). Protein samples were subsequently diluted with sample buffer, heated at 70 °C for 10 minutes. These samples were separated on a 4-20% w/v SDS PAGE gel (BioRad), and transferred to a nitrocellulose membrane (BioRad). This membrane was blocked for 1 hour in AquaBlock™/EIA/WB (EastCoast bio) and incubated in 1:1000 diluted solution of PTEN (Cell signaling, 9552), 1:1000 diluted solution of myosin light chain (Abcam, ab11082), 1:500 diluted solution of phosphorylated myosin light chain (Cell signaling, 3674), 1:1000 diluted solution of Akt (Cell signaling, 9272), 1:1000 diluted solution of phospohorylated Akt (Cell signaling, 9271) and 1:1000 diluted solution of GAPDH (Abcam, ab9485) in blocking solution at 4 °C overnight. After washed (three times for 10 minutes) in TBST (10 mM Tris, pH 8.0 and 0.1% v/v Tween 20), goat anti-rabbit and anti-mouse secondary antibodies for Odyssey® western blotting (Li-cor) were treated. Finally, after washing with TBST, Odyssey® CLx infrared imaging system (Li-cor) was applied to blotting. For quantification, each blot was repeated at least three times.

Time-Lapse Microscopy

Images were acquired after cells were fully attached. For long-term observation, the custom-made MatTek dish integrated with topographically patterned substratum was mounted onto the stage of a motorized inverted microscope (Zeiss Axiovert 200M) equipped with a Cascade 512B II CCD camera that has the environmental chamber containing. Phase-contrast and epi-fluorescent images of cells were automatically recorded using the Slidebook 4.1 (Intelligent Imaging Innovations, Denver, CO) for 5 hours at 10 min intervals.

Tracking Cells

To investigate the migratory behavior on the pattern, we tracked cells manually in every image taken by time lapse by outlining the boundary of each cell. Then, using a custom MATLAB code (The MathWorks, Natick, MA), we obtained the positions of cell centroids as a function of time. The code is accessible in supplementary information. The D/T was defined as the ratio of shortest distance between the initial location of an individual cell and its final location to the length of whole itinerary of the cell during live cell imaging.

Quantification of spatial PI3K translocation

Segmentation of epi-fluorescent images was performed as follows. MATLAB Image Processing Toolbox allows reading the pixel values that describe the intensity in a manually isolated single cell. Hot spots, the regions that have higher intensity value on cell membrane than the average intensity of total pixels in a single cell, were segmented. Then, we grouped each hot spot after cutting off the area below the threshold area for ensuring continuous activation of signal. Based on these groups of hot spots, we acquire the area (A), average intensity (F), and centroid coordinates of each hot spot region to calculate the overall signaling vector within a cell. The position of the hot spot relative to the cell centroid, $x_i = (x_i, y_i)$ was defined by subtracting the coordinates of the cell's centroid from those of its hot spots, i. Its vector, s_i is described by the magnitude equal to the total fluorescence intensity of the spot, (A_iF_i); and the overall signaling vector, S, describing spatial PI3K translocation is the sum of s_i. These vectors indicated the direction of spatial PI3K activation in an individual cell[49]. Then, we averaged all of the signaling vectors of each time point and

calculated the direction of averaged signaling vector of each cell for 5 hours (Supplementary Fig 8a).

$$s_i = A_i F_i \frac{x_i}{\sqrt{x_i^2 + y_i^2}}; \quad S = \sum_{N}^{i=1} s_i$$

Magnetic Twisting Cytometry (MTC)

To quantify stiffness of the living adherent cell, we used MTC as described previously[50,51]. In brief, a functionalized ferrimagnetic microbead bound to the cytoskeleton (CSK) through cell surface integrin receptors was magnetized horizontally and then twisted in a vertically aligned homogenous magnetic field that varied sinusoidally in time. The sinusoidal twisting field causes both a rotation and a pivoting displacement of the bead. As the bead moves, the cell develops internal stresses that in turn resist bead motions. Lateral bead displacements in response to the resulting oscillatory torque were detected via a CCD camera (Orca II-ER, Hamamatsu, Japan) attached to an inverted optical microscope (Leica Microsystems, Bannockburn, IL), and with an accuracy of 5 nm using an intensity-weighted center-of-mass algorithm. We defined the ratio of specific applied torque to lateral bead displacements as the complex elastic modulus of the cell, $g^*(f) = g'(f) + i\,g''(f)$, where g' is the storage modulus (cell stiffness), g'' is the loss modulus (cell friction), and $i^2 = -1$. Cell stiffness and friction are expressed in units of Pascal per nm (Pa/nm). Statistic analyses were performed using unpaired two-tailed Student's *t* tests. To satisfy the normal distribution assumptions, cell stiffness data were square root transformed and confirmed by the Jarque-Bera test.

Immunofluorescence Staining

Cultures were conducted on the nanofabricated coverslip as described above after coating with FN. We fixed with ice-cold 4% paraformaldehyde for 20 minutes, washed two times with phosphate-buffered saline (PBS) and permeablized with 0.1% Triton X-100 in PBS for 5 minutes. After washing with PBS, cultures were blocked by 10% goat-serum for 1 hour, and then incubated with primary antibody against vinculin (1:200, Sigma-Aldrich, V9131) for 3 hours in room temperature. After washing, with secondary antibody for vinculin (1:500), Alexa fluor 594 conjugated phalloidin (1:40, Molecular Probes, A12381) and Hoescht (Invitrogen, 33342), cultures were incubated for 1 hour in room temperature. The slides were mounted with anti-fade reagent (SlowFade gold, Invitrogen) and taken by confocal microscope (Zeiss 510 Meta confocal) with a X63 oil immersion objective (Zeiss, 1.6 NA).

Proliferation assay

1205Lu and SBcl2 cells were plated on the nanofabricated coverslips pre-coated with 10 or 50 μg/ml of FN. After 1 day of culture, cells were immunofluorescently stained with Ki67 (Abcam, ab15580) and Hoescht (Invitrogen, 33342) as described above. Next, we counted all cells and the cells positive for Ki67, a proliferation marker, in sparse and dense post regions on GPDA. Then, the ratios of the number of Ki67-positive cells to that of total cells in each region analyzed were calculated to assess the proliferation rate.

Measurement of Relative Depths of Vinculin-stained Focal Adhesions

Cells with immunofluorescence-stained vinculin were imaged using confocal microscope (Leica SP8) with a X63 oil immersion objective (Zeiss, 1.6 NA), and the Z- direction re-construction was performed with customized MATLAB code (The MathWorks, Natick, MA). The code is accessible in supplementary information. We found the centroid coordinates of the re-constructed vinculin-stained focal adhesions and measured their depths relative to the zero plain level (at the top of the posts) based on the Z-coordinates. Then, we divided the vinculin-marked focal adhesions in individual cells into two groups, depending on their locations corresponding to the local post density, i.e., those in the sparser vs. denser post regions, and averaged their depths within each group. Relative depths were calculated by subtracting the mean depth of the focal adhesions on denser relative to the sparser region in an individual cell; positive relative depth indicates deeper average focal adhesions penetration on the sparser post region than on denser post region.

Scanning Electron Microscopy (SEM)

For scanning electron microscopy, cultured melanoma cells on the graded nano-post density adhesion substrata were washed with phosphate-buffered saline (PBS, pH 7.4, Gibco Invitrogen) and fixed in 3% glutaraldehyde (Sigma-Aldrich) in PBS for 1 hr. After fixation, we rinsed samples in 0.1 M sodium cacodylate for thirty minutes at 4°C and then post-fixed in 2% osmium tetroxide for 1 hr at the same temperature. After a brief D-H_2O rinse, samples were en-bloc stained in 2% aqueous uranyl acetate (0.22 μm filtered) for 1 hr at room temperature in the dark. Following a graded ethanol dehydration cells were critical point dried with liquid CO_2, mounted onto SEM stubs with double stick carbon tape, and sputter coated with 10 nm gold palladium. Samples were viewed and photographed with a LEO FESEM 1530 operating at 1 kV.

Supplementary Material

Refer to Web version on PubMed Central for supplementary material.

Acknowledgement

We thank Dr. Rhoda Alani (Boston University) for sharing melanoma cell lines and Dr. Jin Zhang for sharing plasmids (UCSD); Amanda Pellowe and Dr. Anjelica L Gonzalez (Yale University) for helping SEM imaging; J.P is a recipient of Samsung scholarship. This work was also supported by NIH grant U01CA15578 to A.L and HL107361, U54 CA141868, P50 CA103175 to S.S.A.

References

1. Devreotes P, Janetopoulos C. Eukaryotic chemotaxis: distinctions between directional sensing and polarization. The Journal of biological chemistry. 2003; 278:20445–20448. doi:10.1074/jbc.R300010200 R300010200 [pii]. [PubMed: 12672811]
2. McCarthy JB, Furcht LT. Laminin and fibronectin promote the haptotactic migration of B16 mouse melanoma cells in vitro. The Journal of cell biology. 1984; 98:1474–1480. [PubMed: 6715409]
3. Aznavoorian S, Stracke ML, Krutzsch H, Schiffmann E, Liotta LA. Signal transduction for chemotaxis and haptotaxis by matrix molecules in tumor cells. The Journal of cell biology. 1990; 110:1427–1438. [PubMed: 2324200]

4. Lo CM, Wang HB, Dembo M, Wang YL. Cell movement is guided by the rigidity of the substrate. Biophys J. 2000; 79:144–152. doi:S0006-3495(00)76279-5 [pii] 10.1016/S0006-3495(00)76279-5. [PubMed: 10866943]
5. Li S, Huang NF, Hsu S. Mechanotransduction in endothelial cell migration. J Cell Biochem. 2005; 96:1110–1126. doi:10.1002/jcb.20614. [PubMed: 16167340]
6. Kim DH, Provenzano PP, Smith CL, Levchenko A. Matrix nanotopography as a regulator of cell function. J Cell Biol. 2012; 197:351–360. doi:10.1083/jcb.201108062 jcb.201108062 [pii]. [PubMed: 22547406]
7. Dalby MJ, Riehle MO, Yarwood SJ, Wilkinson CD, Curtis AS. Nucleus alignment and cell signaling in fibroblasts: response to a micro-grooved topography. Exp Cell Res. 2003; 284:274–282. doi:S0014482702000538 [pii]. [PubMed: 12651159]
8. Diehl KA, Foley JD, Nealey PF, Murphy CJ. Nanoscale topography modulates corneal epithelial cell migration. J Biomed Mater Res A. 2005; 75:603–611. doi:10.1002/jbm.a.30467. [PubMed: 16106433]
9. Kaiser JP, Reinmann A, Bruinink A. The effect of topographic characteristics on cell migration velocity. Biomaterials. 2006; 27:5230–5241. doi:S0142-9612(06)00528-X [pii] 10.1016/j.biomaterials.2006.06.002. [PubMed: 16814858]
10. Teixeira AI, et al. The effect of environmental factors on the response of human corneal epithelial cells to nanoscale substrate topography. Biomaterials. 2006; 27:3945–3954. doi:10.1016/j.biomaterials.2006.01.044. [PubMed: 16580065]
11. Kim DH, et al. Mechanosensitivity of fibroblast cell shape and movement to anisotropic substratum topography gradients. Biomaterials. 2009; 30:5433–5444. doi:10.1016/j.biomaterials.2009.06.042 S0142-9612(09)00647-4 [pii]. [PubMed: 19595452]
12. Kim DH, et al. Guided Cell Migration on Microtextured Substrates with Variable Local Density and Anisotropy. Adv Funct Mater. 2009; 19:1579–1586. doi:10.1002/adfm.200990041. [PubMed: 20046799]
13. Sochol RD, Higa AT, Janairo RRR, Li S, Lin LW. Unidirectional mechanical cellular stimuli via micropost array gradients. Soft Matter. 2011; 7:4606–4609. doi:Doi 10.1039/C1sm05163f.
14. Miller AJ, Mihm MC Jr. Melanoma. N Engl J Med. 2006; 355:51–65. doi:355/1/51 [pii] 10.1056/NEJMra052166. [PubMed: 16822996]
15. Kessenbrock K, Plaks V, Werb Z. Matrix metalloproteinases: regulators of the tumor microenvironment. Cell. 2010; 141:52–67. doi:10.1016/j.cell.2010.03.015 S0092-8674(10)00288-6 [pii]. [PubMed: 20371345]
16. Mott JD, Werb Z. Regulation of matrix biology by matrix metalloproteinases. Current opinion in cell biology. 2004; 16:558–564. doi:10.1016/j.ceb.2004.07.010. [PubMed: 15363807]
17. Gaggioli C, et al. Tumor-derived fibronectin is involved in melanoma cell invasion and regulated by V600E B-Raf signaling pathway. The Journal of investigative dermatology. 2007; 127:400–410. doi:10.1038/sj.jid.5700524. [PubMed: 16960555]
18. Kaariainen E, et al. Switch to an invasive growth phase in melanoma is associated with tenascin-C, fibronectin, and procollagen-I forming specific channel structures for invasion. The Journal of pathology. 2006; 210:181–191. doi:10.1002/path.2045. [PubMed: 16924594]
19. Ushiki T. Collagen fibers, reticular fibers and elastic fibers. A comprehensive understanding from a morphological viewpoint. Archives of histology and cytology. 2002; 65:109–126. [PubMed: 12164335]
20. Smith LA, Ma PX. Nano-fibrous scaffolds for tissue engineering. Colloids and surfaces. B, Biointerfaces. 2004; 39:125–131. doi:10.1016/j.colsurfb.2003.12.004. [PubMed: 15556341]
21. Chhabra ES, Higgs HN. The many faces of actin: matching assembly factors with cellular structures. Nature cell biology. 2007; 9:1110–1121. doi:ncb1007-1110 [pii] 10.1038/ncb1007-1110. [PubMed: 17909522]
22. Charras GT, Hu CK, Coughlin M, Mitchison TJ. Reassembly of contractile actin cortex in cell blebs. The Journal of cell biology. 2006; 175:477–490. doi:10.1083/jcb.200602085. [PubMed: 17088428]

23. Morone N, et al. Three-dimensional reconstruction of the membrane skeleton at the plasma membrane interface by electron tomography. The Journal of cell biology. 2006; 174:851–862. doi:10.1083/jcb.200606007. [PubMed: 16954349]
24. Gilden J, Krummel MF. Control of cortical rigidity by the cytoskeleton: emerging roles for septins. Cytoskeleton. 2010; 67:477–486. doi:10.1002/cm.20461. [PubMed: 20540086]
25. Thiery JP, Acloque H, Huang RY, Nieto MA. Epithelial-mesenchymal transitions in development and disease. Cell. 2009; 139:871–890. doi:10.1016/j.cell.2009.11.007. [PubMed: 19945376]
26. Fabry B, et al. Scaling the microrheology of living cells. Physical review letters. 2001; 87:148102. [PubMed: 11580676]
27. An SS, Laudadio RE, Lai J, Rogers RA, Fredberg JJ. Stiffness changes in cultured airway smooth muscle cells. Am J Physiol Cell Physiol. 2002; 283:C792–801. doi:10.1152/ajpcell.00425.2001. [PubMed: 12176736]
28. Wettschureck N, Offermanns S. Rho/Rho-kinase mediated signaling in physiology and pathophysiology. Journal of molecular medicine. 2002; 80:629–638. doi:10.1007/s00109-002-0370-2. [PubMed: 12395147]
29. Riento K, Ridley AJ. Rocks: multifunctional kinases in cell behaviour. Nature reviews. Molecular cell biology. 2003; 4:446–456. doi:10.1038/nrm1128. [PubMed: 12778124]
30. Wilkinson S, Paterson HF, Marshall CJ. Cdc42-MRCK and Rho-ROCK signalling cooperate in myosin phosphorylation and cell invasion. Nature cell biology. 2005; 7:255–261. doi:10.1038/ncb1230. [PubMed: 15723050]
31. Innocenti M, et al. Phosphoinositide 3-kinase activates Rac by entering in a complex with Eps8, Abi1, and Sos-1. The Journal of cell biology. 2003; 160:17–23. doi:10.1083/jcb.200206079. [PubMed: 12515821]
32. Welch HC, Coadwell WJ, Stephens LR, Hawkins PT. Phosphoinositide 3-kinase-dependent activation of Rac. FEBS letters. 2003; 546:93–97. [PubMed: 12829242]
33. Levine H, Kessler DA, Rappel WJ. Directional sensing in eukaryotic chemotaxis: a balanced inactivation model. Proc Natl Acad Sci U S A. 2006; 103:9761–9766. doi:10.1073/pnas.0601302103. [PubMed: 16782813]
34. Janetopoulos C, Firtel RA. Directional sensing during chemotaxis. FEBS Lett. 2008; 582:2075–2085. doi:10.1016/j.febslet.2008.04.035. [PubMed: 18452713]
35. Yamada KM, Araki M. Tumor suppressor PTEN: modulator of cell signaling, growth, migration and apoptosis. Journal of cell science. 2001; 114:2375–2382. [PubMed: 11559746]
36. Wu H, Goel V, Haluska FG. PTEN signaling pathways in melanoma. Oncogene. 2003; 22:3113–3122. doi:10.1038/sj.onc.1206451. [PubMed: 12789288]
37. Levchenko A, Iglesias PA. Models of eukaryotic gradient sensing: application to chemotaxis of amoebae and neutrophils. Biophys J. 2002; 82:50–63. doi:10.1016/S0006-3495(02)75373-3. [PubMed: 11751295]
38. Nogueira C, et al. Cooperative interactions of PTEN deficiency and RAS activation in melanoma metastasis. Oncogene. 2010; 29:6222–6232. doi:10.1038/onc.2010.349. [PubMed: 20711233]
39. Hwang PH, et al. Suppression of tumorigenicity and metastasis in B16F10 cells by PTEN/MMAC1/TEP1 gene. Cancer Lett. 2001; 172:83–91. [PubMed: 11595133]
40. Jeon H, et al. Directing cell migration and organization via nanocrater-patterned cell-repellent interfaces. Nature materials. 2015 doi:10.1038/nmat4342.
41. Saez A, Ghibaudo M, Buguin A, Silberzan P, Ladoux B. Rigidity-driven growth and migration of epithelial cells on microstructured anisotropic substrates. Proceedings of the National Academy of Sciences of the United States of America. 2007; 104:8281–8286. doi:10.1073/pnas.0702259104. [PubMed: 17488828]
42. Ghassemi S, et al. Cells test substrate rigidity by local contractions on submicrometer pillars. Proceedings of the National Academy of Sciences of the United States of America. 2012; 109:5328–5333. doi:10.1073/pnas.1119886109. [PubMed: 22431603]
43. Kim P, et al. Fabrication of nanostructures of polyethylene glycol for applications to protein adsorption and cell adhesion. Nanotechnology. 2005; 16:2420–2426. doi:10.1088/0957-4484/16/10/072 S0957-4484(05)01664-8 [pii]. [PubMed: 20818029]

44. Ananthanarayanan B, Fosbrink M, Rahdar M, Zhang J. Live-cell molecular analysis of Akt activation reveals roles for activation loop phosphorylation. The Journal of biological chemistry. 2007; 282:36634–36641. doi:10.1074/jbc.M706227200. [PubMed: 17928291]
45. Weiger MC, et al. Spontaneous phosphoinositide 3-kinase signaling dynamics drive spreading and random migration of fibroblasts. Journal of cell science. 2009; 122:313–323. doi:10.1242/jcs.037564 jcs.037564 [pii]. [PubMed: 19126672]
46. Kim P, et al. Fabrication of nanostructures of polyethylene glycol for applications to protein adsorption and cell adhesion. Nanotechnology. 2005; 16:2420–2426. doi:10.1088/0957-4484/16/10/072 S0957-4484(05)01664-8 [pii]. [PubMed: 20818029]
47. Jeong HE, Kwak R, Khademhosseini A, Suh KY. UV-assisted capillary force lithography for engineering biomimetic multiscale hierarchical structures: From lotus leaf to gecko foot hairs. Nanoscale. 2009; 1:331–338. doi:10.1039/b9nr00106a. [PubMed: 20648269]
48. Ananthanarayanan B, Fosbrink M, Rahdar M, Zhang J. Live-cell molecular analysis of Akt activation reveals roles for activation loop phosphorylation. The Journal of biological chemistry. 2007; 282:36634–36641. doi:10.1074/jbc.M706227200. [PubMed: 17928291]
49. Weiger MC, et al. Spontaneous phosphoinositide 3-kinase signaling dynamics drive spreading and random migration of fibroblasts. Journal of cell science. 2009; 122:313–323. doi:10.1242/jcs.037564. [PubMed: 19126672]
50. Thiery JP, Acloque H, Huang RY, Nieto MA. Epithelial-mesenchymal transitions in development and disease. Cell. 2009; 139:871–890. doi:10.1016/j.cell.2009.11.007. [PubMed: 19945376]
51. Fabry B, et al. Scaling the microrheology of living cells. Physical review letters. 2001; 87:148102. [PubMed: 11580676]

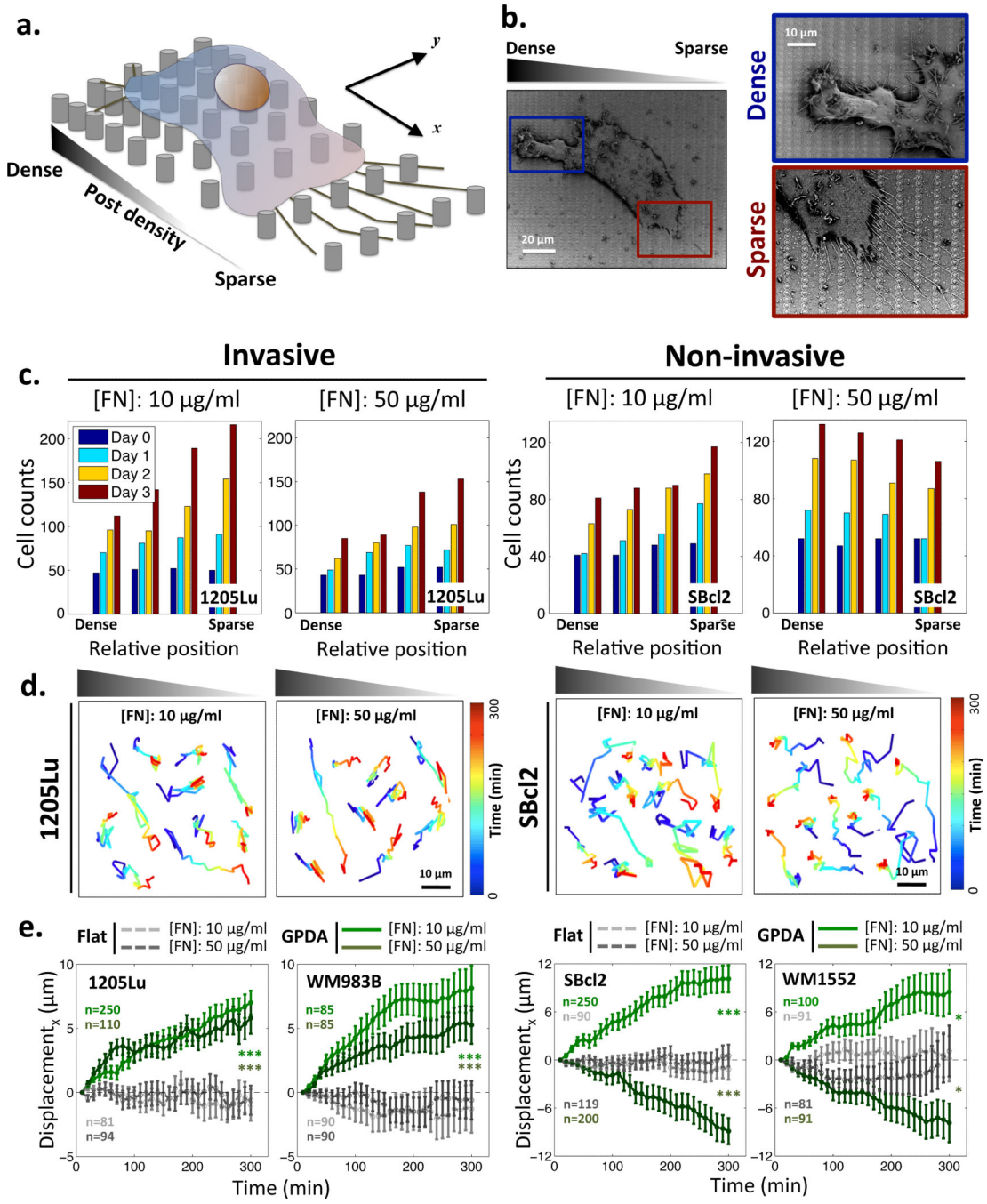

Figure 1.

Topotactic migration of melanoma cells guided by the gradient of the post density and pre-coated ECM density. (a) Schematic of a cell culture on the graded post substratum; (b) SEM images of a 1205Lu melanoma cell cultured on the graded post substratum. Magnified areas focus on different formations of filopodia in the denser (blue box) vs. sparser post region (red box); (c) Changes in the number of cells as a function of time and the post density for 1205Lu cells and SBcl2 cells on GPDA, pre-coated with 10 μg/ml and 50 μg/ml of FN; (d) Trajectories of 1205Lu and SBcl2 cell migration on the gradient of post density pre-coated

10 μg/ml and 50 μg/ml of FN; (e) Biased migration of invasive (1205Lu and WM983B) and non-invasive (SBcl2 and WM1552) melanoma cells evaluated as the average shift from the initial position on 10 μg/ml and 50 μg/ml of FN for 5 hours in the direction parallel to the gradient of post density. Positive values indicate the migration from denser-to sparser post regions. * = Statistical significance of biased directional migration on GPDA compared with migration on flat substrata. *P<0.05 and ***P<0.005 and all paired two-sample Student's t-test. All error bars are S.E.M.

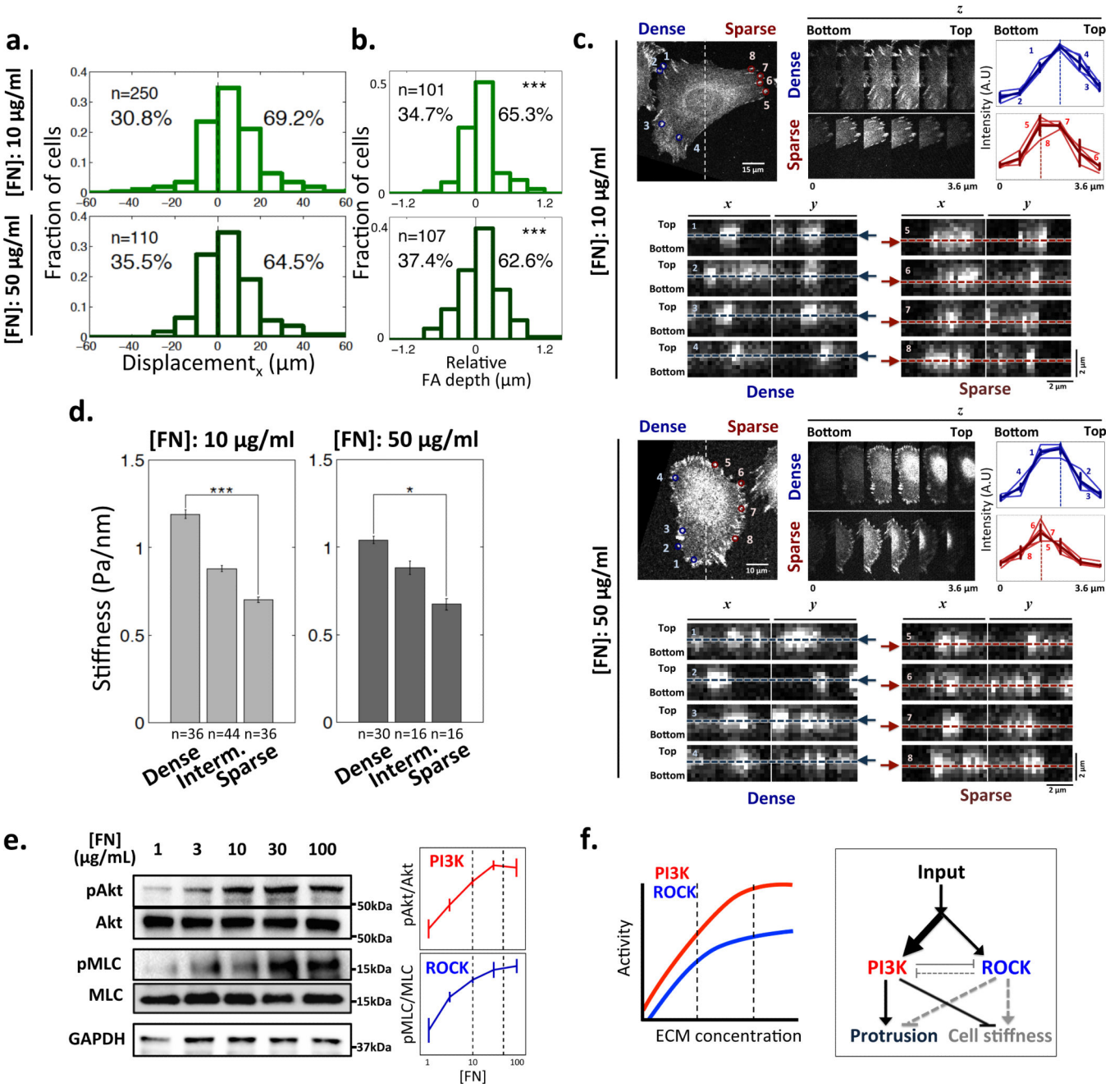

Figure 2.

Correlation of the topotactic migration direction and cell stiffness as a function of the local post density. (a) Fractions of 1205Lu cell displacements in *x* direction for 5 hours on 10 μg/ml FN and 50 μg/ml FN pre-coated GPDA. Positive values indicate the migration from denser-to sparser post regions; (b) The fractions of 1205Lu cells that have relatively deeper FAs penetration into the substratum in the sparser vs. denser post array zones of 10 μg/ml FN and 50 μg/ml FN coated GPDA (see panel (c) for examples of the image analysis). * = Statistical significance of deviation from zero mean which indicates vertically even distribution of FAs in individual cells. ***P<0.005. Wilcoxon signed rank test for zero

mean. (c) Confocal images of vinculin-stained cells showing differential vertical protrusions of 1205Lu cells, as a function of the post density, on indicated [FN]. For each [FN], we analyzed the depths of FAs, as represented by vinculin staining intensity, located in the denser region, 1-4 (blue), and in the sparser region, 5-8 (red). In the top right panel, we show z-series images and analysis of signal intensity of corresponding FAs in z-direction; FAs in denser regions show peak intensity (dashed lines) at higher z-distance measured from the glass bottom (the z-position of 0), than those in sparser regions. In the bottom panels, x-z and y-z projections of FAs are shown with respect to the glass bottom (with the maximum vinculin staining positions determined in the top panels marked with dashed lines and arrows) (d) Dependence of cell stiffness on the local post density on 10 μg/ml FN and 50 μg/ml FN coated GPDAs, with the gradient range divided into three equally sized zones of the different local post densities. * = Statistical significance between the values on the dense vs. sparse post density zones. *P<0.05, **P<0.01 and ***P<0.005. All paired two-sample Student's t-test. All error bars are S.E.M. (e) ECM-stimulated ROCK and PI3K activity in 1205Lu cells evaluated by immunoblotting of their substrates: Akt and MLC, All error bars are S.E.M (n=3); (f) A schematic depiction of ECM-triggered signaling pathway activities in 1205Lu cells shown in panel (e) and their effect on membrane protrusion and cell stiffness, assuming relative dominance of the PI3K pathway, which leads to a decrease in cell stiffness (and thus increasing substratum penetration) with increasing ECM contact.

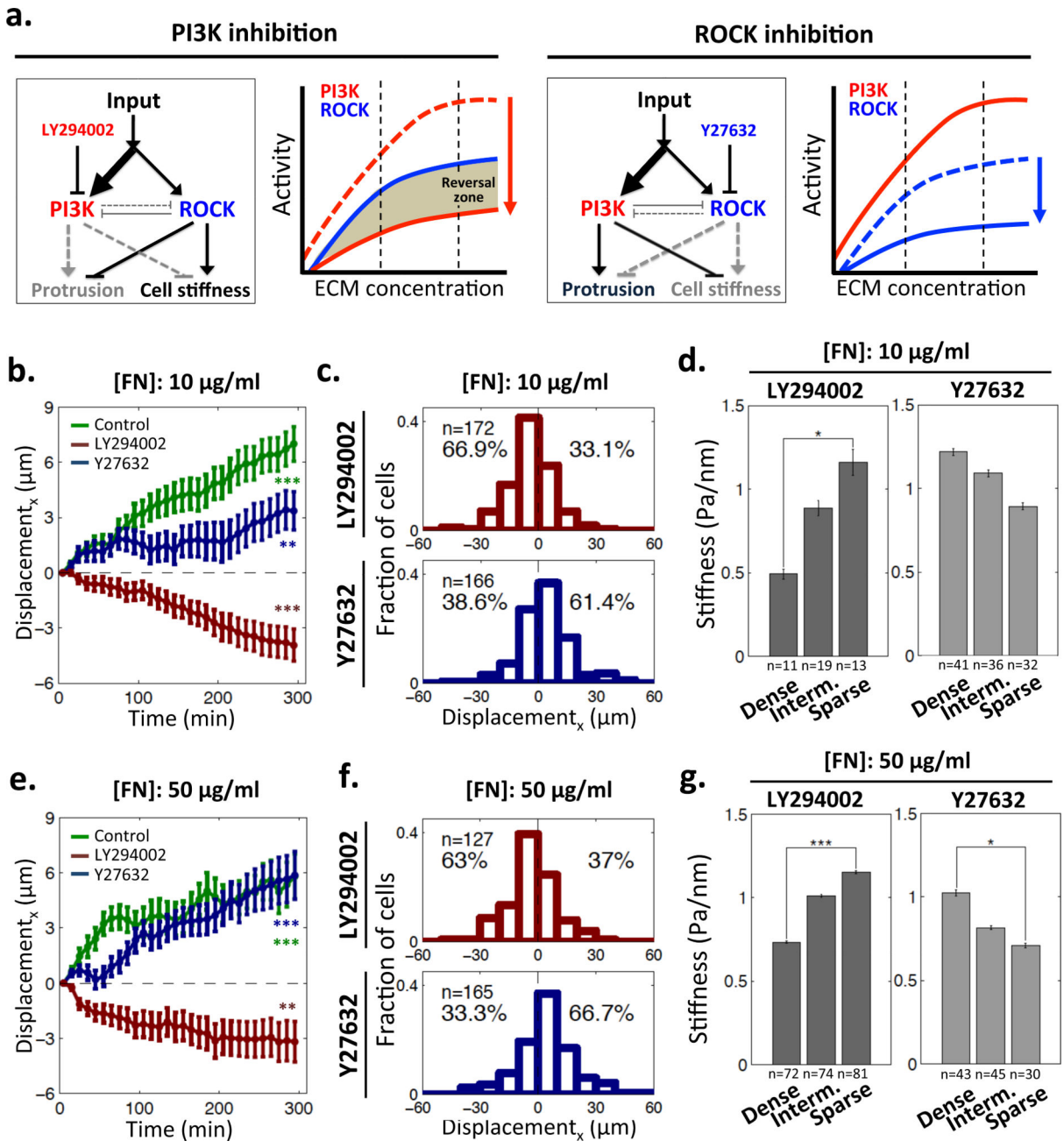

Figure 3.

Modulation of topotaxis direction of 1205Lu cells by perturbations of PI3K and ROCK signaling. (a) Predicted changes of activity of the signaling network regulating cell stiffness of 1205Lu cells by pharmacological inhibition of PI3K (LY294002, red arrow) and ROCK (Y27632, blue arrow). PI3K inhibition is predicted to generate a 'reversal zone': the ECM density range where ROCK activity becomes dominant over PI3K activity, which results in a reversal the direction of the topotactic cell migration. (b,e) Cell displacements in the direction parallel to post density gradient on 10 μg/ml FN pre-coated GPDA (b) and 50 μg/ml FN pre-coated GPDA for 5 hours (e). * = Statistical significance of the biased deviation from the zero mean in the *x*-direction. **P<0.01 and ***P<0.005. Wilcoxon

signed rank test for zero mean. All error bars are S.E.M.; (c,f) The distributions of topotactic cell displacements on 10 μg/ml FN pre-coated GPDA (c) and 50 μg/ml FN pre-coated GPDA (f) following treatment with a ROCK inhibitor, (5μM of Y27632) and a PI3K inhibitor (10μM of LY294002); (d,g) Modulation of cell stiffness dependence on the post density of 10 μg/ml FN (d) and 50 μg/ml FN coated GPDA (g) following PI3K and ROCK signaling perturbations. * = Statistical significance of the difference between the values on the dense vs. sparse regions. *P<0.05, **P<0.01 and ***P<0.005. All paired two-sample Student's t-test. All error bars are S.E.M.

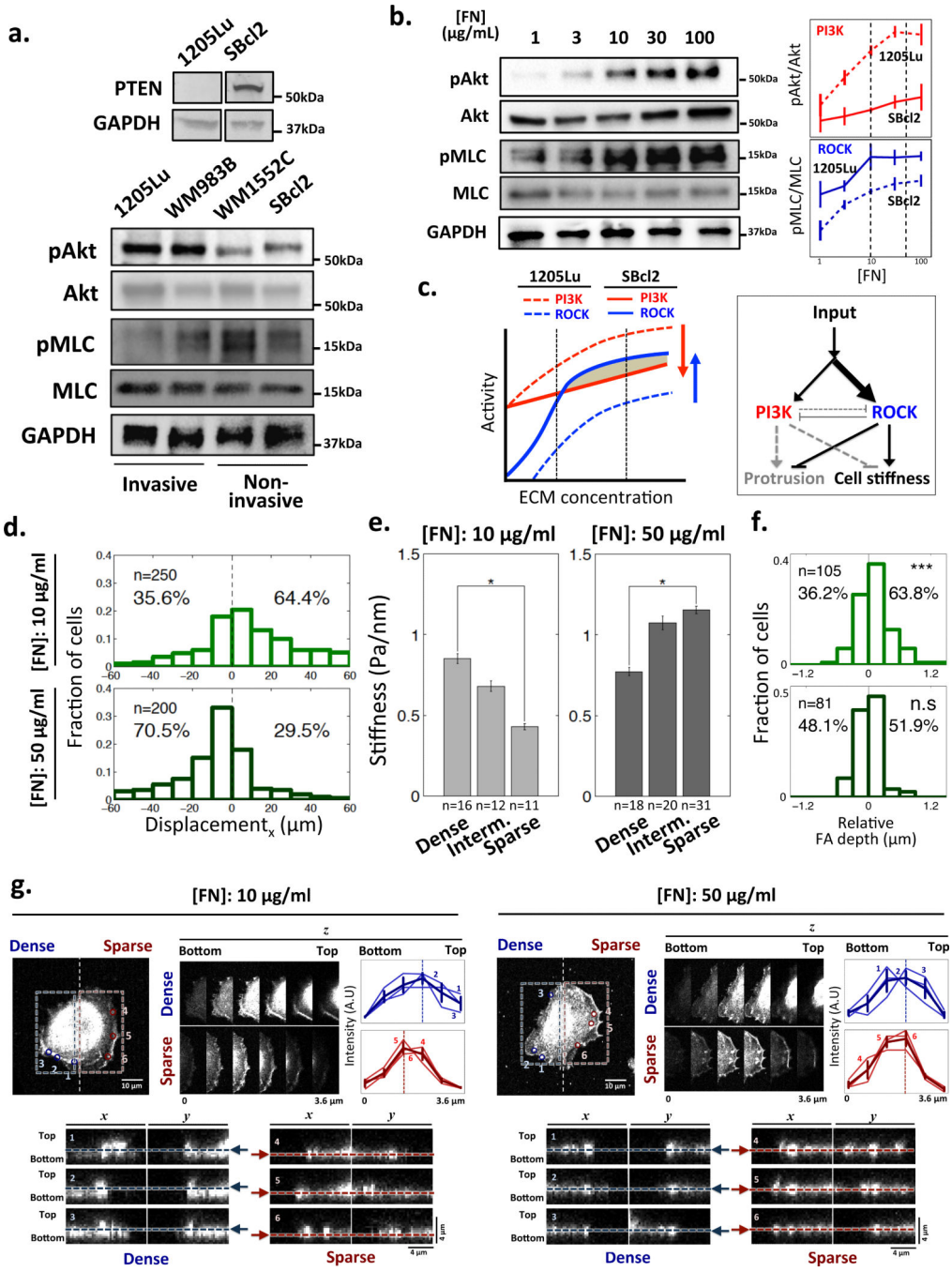

Figure 4.

Functional PTEN in non-invasive SBcl2 modulates its topotactic properties accounting for the responses shown in Fig. 1. (a) Non-invasive SBcl2 melanoma but not invasive 1205Lu cells express PTEN, a PI3K antagonist. Non-invasive melanoma cell lines, SBcl2 and WM1552C, display lower PI3K activity and higher ROCK activity vs. invasive 1205Lu and WM983B cell lines on GPDA coated with 1 μg/ml of FN; (b) Dependence of the PI3K and ROCK activity in SBcl2 cells on the ECM density measured by assaying their substrates, Akt and MLC correspondingly. The data were quantified and normalized using the analysis

in panel (a) to show the relative PI3K and ROCK activities in SBcl2 (solid) and 1205Lu (dashed) cell lines. All error bars are S.E.M; (c) PI3K and ROCK signaling pathway activities in SBcl2 (solid) and 1205Lu (dashed) cell lines, inferred from panel (b), showing the predicted change in the balance of the relative PI3K and ROCK signaling activities and the resulting switch in the topotaxis directionality. This change in the activity balance is also schematically depicted in the diagram on the right; (d) The distributions of topotactic displacements of SBcl2 cells on 10 μg/ml FN and 50 μg/ml FN-coated GPDA over the course of 5 hours; (e) Reversal of the SBcl2 cell stiffness dependence on the post density in cells cultured on 50 μg/ml vs. 10 μg/ml FN coating density on GPDA. * = Statistical significance between the values on dense vs. sparse region. *$P<0.05$ and all paired two-sample Student's t-test. All error bars are S.E.M. (f) The fractions of SBcl2 cells that have relatively deeper FAs penetration into the substratum in the sparser vs. denser post array zones on 10 μg/ml FN and 50 μg/ml FN coated GPDA. * = Statistical significance of the deviation from the zero mean. n.s = no significance and ***$P<0.005$. Wilcoxon signed rank test for zero mean. (g) Confocal images showing differential vertical protrusions of SBcl2 cells depending on post density and ECM density. The analysis is equivalent to that shown in Fig. 2c.

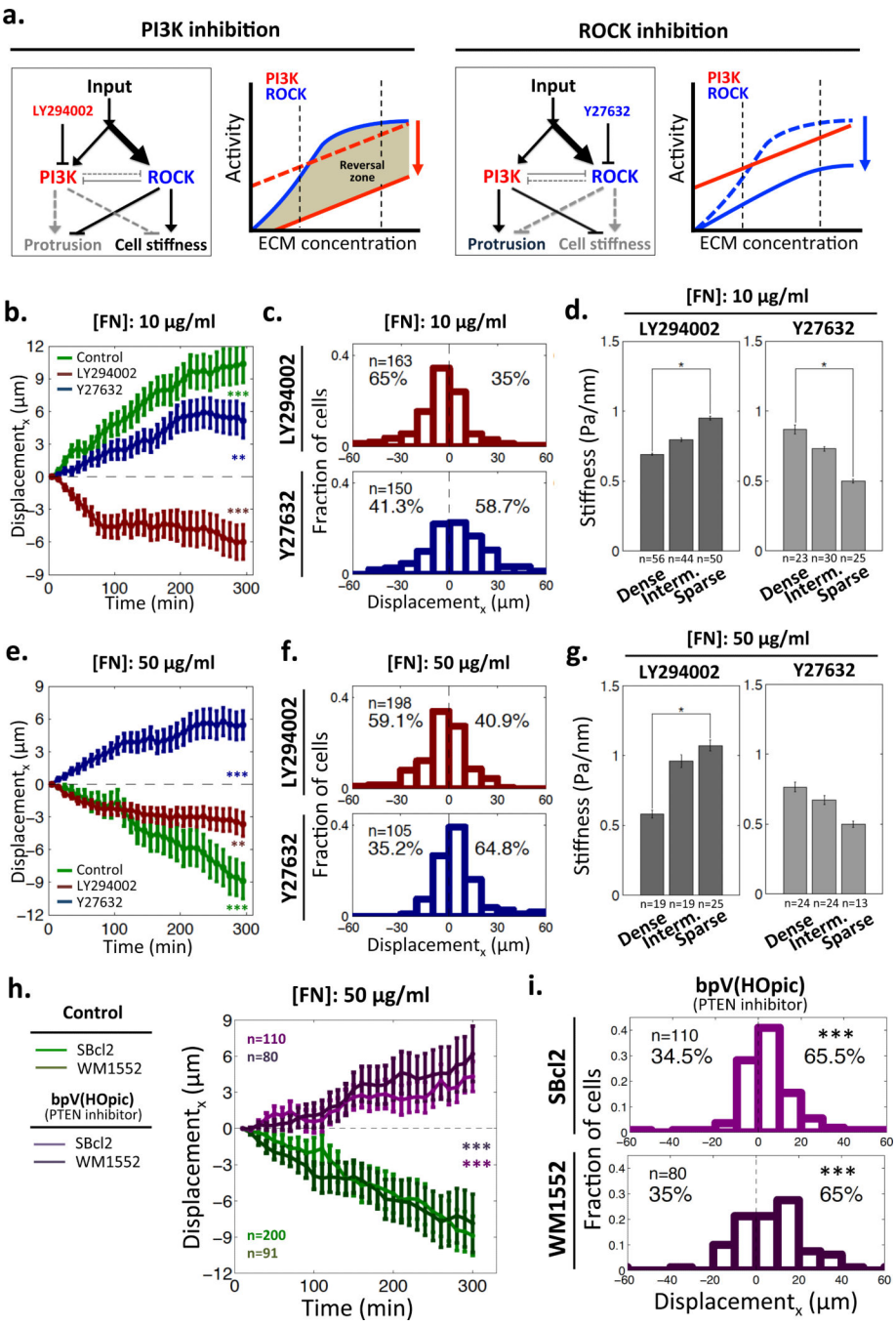

Figure 5.

Modulation of topotaxis direction of SBcl2 cells by perturbations of PI3K and ROCK signaling. (a) Predicted changes of activity of the signaling network regulating cell stiffness of SBcl2 cells by pharmacological inhibition of PI3K (LY294002, red arrow) and ROCK (Y27632, blue arrow). PI3K inhibition is predicted to extend the reversal of the balance between PI3K and ROCK activities to the whole ECM density range in contrast to ROCK inhibition removing the reversal; (b,e) SBcl2 cell displacements in the direction parallel to post density gradient on 10 μg/ml FN pre-coated GPDA (b) and 50 μg/ml FN pre-coated

GPDA examined for 5 hours (e). * = Statistical significance of the biased deviation from the zero mean in the *x*-direction. **P<0.01 and ***P<0.005. Wilcoxon signed rank test for the zero mean. All error bars are S.E.M.; (c,f) The distributions of topotactic SBcl2 cell displacements on 10 μg/ml FN pre-coated GPDA (c) and 50 μg/ml FN pre-coated GPDA (f) following treatment with a ROCK inhibitor, (5μM of Y27632) and a PI3K inhibitor (10μM LY294002); (d,g) Modulation of cell stiffness dependence on the post density of 10 μg/ml FN (d) and 50 μg/ml FN coated GPDA (g) following PI3K and ROCK signaling perturbations. * = Statistical significance between the values on the dense vs. sparse regions. *P<0.05 and all paired two-sample Student's t-test. All error bars are S.E.M. (h) Modulation of topotaxis direction of non-invasive melanoma cells cultured on GPDA pre-coated with a high FN density, following inhibition of PTEN. SBcl2 and WM1552 cell displacements in the direction parallel to post density gradient on GPDA pre-coated with 50 μg/ml FN and examined for 5 hours following treatment with 100 nM of bpV(HOpic), a PTEN inhibitor. * = Statistical significance of difference in displacement in the x-direction between with and without drug. ***P<0.005. All paired two-sample Student's t-tests. All error bars are S.E.M. (i) The distributions of topotactic SBcl2 and WM1552 cell displacements measured in (h). * = Statistical significance of the biased deviation from the zero mean in the x-direction. ***P<0.005. Wilcoxon signed rank test for the zero mean.

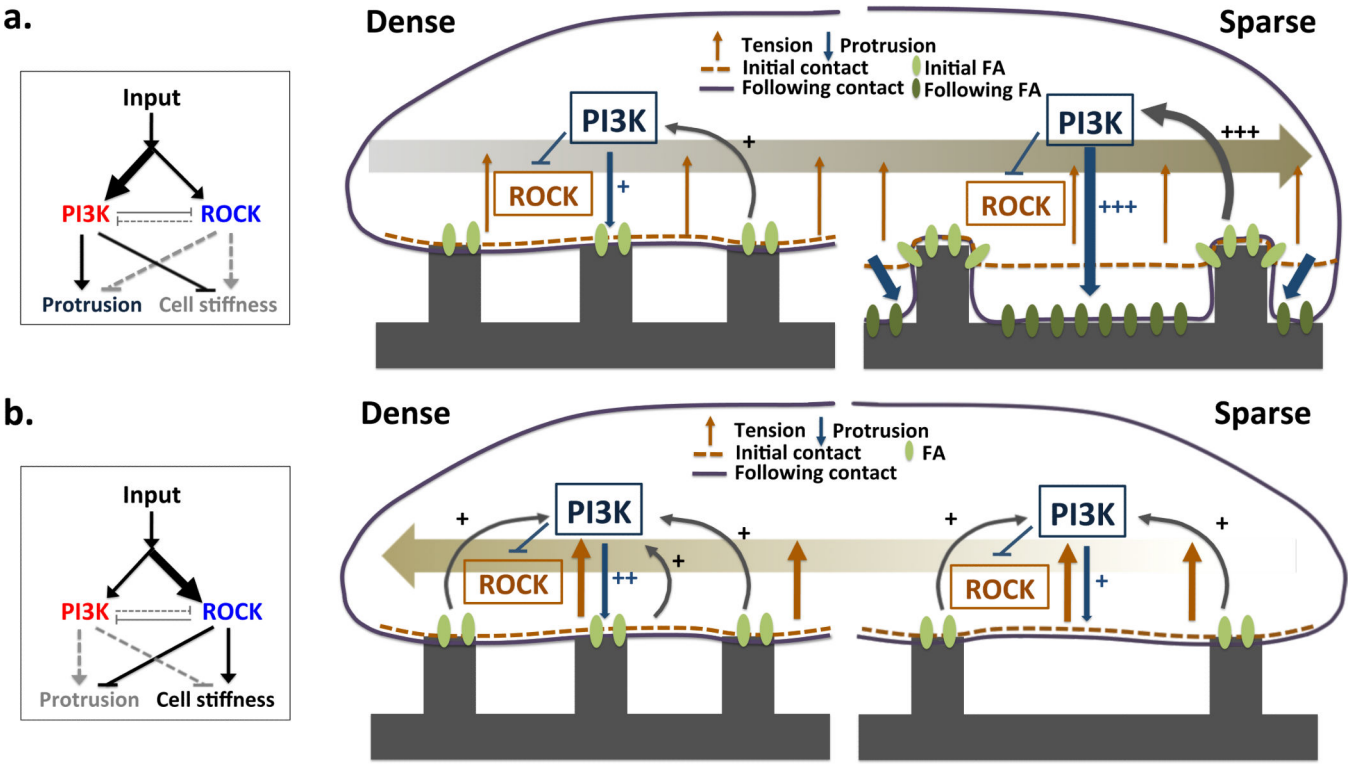

Figure 6.

A schematic graphic model of the topotaxis in invasive and non-invasive cells. The directionality of topotactic migration depends on differential conformity of cellular membrane to local topographic structure. The degree of conformity depends on the cell rigidity, which in turn is controlled by the interplay between two ECM activated signaling pathways: PI3K-Akt increasing the degree of conformity and matrix penetration and ROCK-MLCK decreasing the degree of conformity. The balance between the activities of these pathways can be determined by the local ECM signaling input or genetic changes affecting these pathways, and can be modulated by pharmacological perturbations. The relatively higher activity of the PI3K-Akt pathway in the invasive melanoma cells (a) can lead to differential penetration of the matrix and lead to a higher matrix contact in the sparser vs. denser matrix zones, generating bias for migration from the denser to sparser matrix density. In the other hand, at high enough ECM signaling inputs, the relatively higher activity of the ROCK-MLCK pathway in noninvasive melanoma cells limits cell penetration into the matrix, leading to haptotactic migration up the density gradient (b).